Enhanced Doppler reflectometry power response: physical optics and 2D full wave modelling

J R Pinzón[1,2,3], T Happel[1], E Blanco[4], G D Conway[1], T Estrada[4] and U Stroth[1,2]

[1] Max-Plank-Institute für Plasmaphysik, D-85748 Garching, Germany

[2] Physics Department E28, Technische Universität München, D-85748 Garching, Germany

[3] Departamento de Física, Universidad Carlos III de Madrid, 29811 Leganés, Madrid, Spain

[4] Laboratorio Nacional de Fusión, CIEMAT, 28040 Madrid, Spain

E-mail: jpinzon@ipp.mpg.de

August 2016

Abstract. The power response of a Doppler reflectometer is investigated by means of the physical optics model, a simple model which considers basic scattering processes at the reflection layer. Apart from linear and saturated scattering regimes, non-linear regimes with an enhanced backscattered power are found. The different regimes are characterized and understood based on analytical calculations.

The power response is also studied with 2D full wave simulations, where the enhanced backscattered power regimes are also found in qualitative agreement with the physical optics results. The ordinary and extraordinary mode are compared for the same angle of incidence, concluding that ordinary mode is better suited for Doppler reflectometry turbulence level measurements due to the linearity of its response.

The scattering efficiency is studied and a first approximation to describe it is proposed. At the end, the application of the physical optics results to experimental data analysis is discussed, in particular a formula to assess the linearity of Doppler reflectometry measurements is provided.

1. Introduction

Scattering of electromagnetic waves has been widely used to study turbulence in fusion plasmas [1, 2, 3, 4, 5]. In particular, Doppler reflectometry (DR) uses an oblique microwave beam and studies the backscattered signal due to the turbulence at the cut-off layer. This can provide experimental data on the density turbulence amplitude and its propagation velocity, both important elements for studies of plasma dynamics and performance [6].

Doppler reflectometry has been shown to be a useful diagnostic as it provides radially localized, and perpendicular wavenumber ($k_\perp$) resolved measurements [7], furthermore the Doppler frequency shift of the backscattered signal is proportional

to the perpendicular flow and hence the radial electric field assuming that the phase velocity is small against the $E \times B$ drift velocity, $v_{\rm ph} \ll v_{E\times B}$. Using such properties, $k_\perp$-spectra [8, 9, 10, 11], E_r-profiles [7, 9, 12, 13] and the dynamics of turbulence under different conditions [14, 15] have been studied. Moreover the radial structure of the turbulence can be studied by using two Doppler reflectometer channels simultaneously [16], which is known as radial correlation Doppler reflectometry.

However, it has been observed in simulations [17, 18], experiments [10] and theory [19, 20], that a non-linear response of the reflectometer is involved, which makes the interpretation of data and $k_\perp$-spectra challenging. The measured spectral indices are small [10] and sometimes the spectra are even flat, in disagreement with gyrokinetic simulations. This spectral flattening is believed to be due to a non-linear saturation of the reflectometer signal.

The response of DR has been studied using simplified models such as the Physical Optics (PO) [21], which simulates the scattering at the cutoff as the scattering of electromagnetic waves by a corrugated reflecting surface. This model can be considered a first approximation to the problem which neglects any scattering away from the cutoff. Nevertheless it has been able to describe qualitatively several of the effects observed in the experiments [21, 22, 23].

Nowadays DR is widely modelled via 2D full wave simulations (2DFW) [17, 18, 24, 25], which provide a full solution to the Maxwell equations in a plasma and therefore contain all the relevant physics. They have recovered the effects observed in the experiments [10], and have been useful for direct comparisons between gyrokinetic simulations and experimental reflectometry data. However, the fact that 2DFW are computational demanding for systematic scans of parameters, and since the plasma is hidden in the currents involved in the codes and the solution is achieved just by numerical integration, the physical understanding which can be gained is limited.

Analytic solutions to the reflectometry problem have been developed [19, 20]. They have contributed considerably to the understanding of the physical processes involved, e.g. linear and non-linear response and poor-localized forward scattering. However they are still limited to special conditions regarding the density profile, polarization and turbulence level. In particular for DR an ordinary mode linear [19] and non-linear [20] theories are available, in the weak and strong phase modulation regime of the probing wave, respectively. However the response of DR at the transition between both regimes is not clear yet. The present paper investigates this region.

In this paper we study the power response of Doppler reflectometry by means of PO and 2D full wave simulations. In Sec. 2 we explain and apply the PO model, in Sec. 3 the power response is studied analytically under this approximation and the scattering process behind is understood. In Sec. 4, the Doppler reflectometry power response is modelled using 2D full wave simulation for the ordinary(O) and the extraordinary(X) mode. Later on the applicability of PO to Doppler reflectometry is discussed and its capability as a reliable modelling tool is assessed. Finally in Sec. 5, the application of the results here obtained to experimental data analysis is discussed.

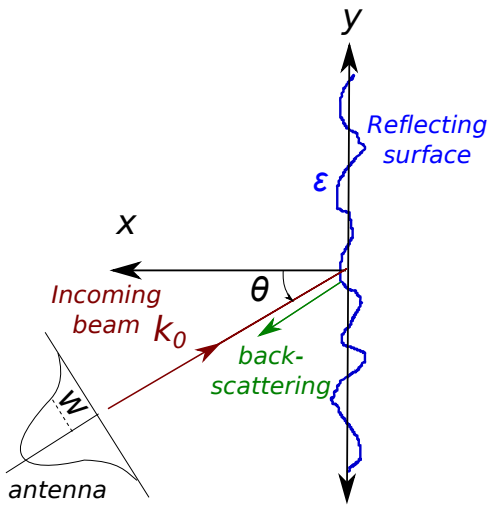

Figure 1. Schematic of the PO model geometry. A corrugated reflecting surface along the y-axis is characterized by the displacement $\varepsilon(y)$ in the x-direction. An incoming paraxial Gaussian beam with wave number k_0 is scattered at the surface. The angle of incidence with respect to the x-axis is θ and the beam waist is w.

2. Physical Optics

The Physical Optics theory was originally developed for studying the scattering of waves by rough surfaces [26]. It has been extensively applied in different fields as oceanology [27], geology [28], meteorology [29] i.e. where the surfaces are characterized by their scattering properties. The original theory has been extended [30, 31, 32] to satisfy specific conditions of such applications.

The original theory [26] was applied for the first time for DR modelling in [21], based on the idea of a roughness of the cutoff layer due to density turbulence in fusion plasmas. It was introduced as a simple modelling tool, which makes strong assumptions such as the slab approximation and the omission of any plasma-wave interaction far from the cutoff. Consequently, it is not meant to give a complete description of DR. Nevertheless, as will be shown later, it can describe the problem investigated with sufficient accuracy.

2.1. Original Model

The geometry of the system and the quantities are shown schematically in Fig. 1. The original model [21] assumes a corrugated reflecting surface along the y-direction characterized by $\varepsilon(y)$, which gives its displacement in x-direction from the mean surface. This rough surface scatters an incoming paraxial Gaussian beam with wavenumber $k_0 = 2\pi/\lambda_0$ and an incidence angle θ, where λ_0 is the vacuum wavelength of the incoming wave and θ is measured with respect to the normal to the mean surface. Invariance along the z-axis is assumed. PO provides the backscattered normalized electric field V given

by,

$$V = \int \mathrm{d}y \, \exp\left(-\frac{y^2\cos^2\theta}{w^2} + i2k_0 y\sin\theta\right)\exp(-i2k_0\varepsilon\cos\theta)(\varepsilon'\sin\theta - \cos\theta)$$
$$\times\left[\int \mathrm{d}y \, \exp\left(-\frac{y^2}{w^2}\right)\right]^{-1}, \tag{1}$$

where w is the beam waist at the surface and $\varepsilon' = \mathrm{d}\varepsilon/\mathrm{d}y$. The backscattered electric field is normalized to the reflected electric field from the a smooth surface at perpendicular incidence, thus V is equivalent to the scattering coefficient in [21].

Equation 1 is deduced by solving the Helmholtz integral in the far field and by applying the Kirchhoff approximation [26]. The last requires the corrugation amplitude $|\varepsilon|$ to be small compared to the wavelength λ_0, this imposes a limitation on the application range of the model which will be discussed in Sec. 3.1 Apart from its application to large fusion plasmas where the slab approximation applies, the PO model can be extended to more general geometries [33].

PO can be applied to Doppler reflectometry assuming that ε is related to the the density fluctuations at the cut-off layer. The x- and y-directions can be considered as radial and poloidal directions, respectively, while the z-axis is taken parallel to the magnetic field. Since the turbulence evolves slowly in time (μs) compared with the probing wave time scale (ns), the previous integral can be solved at each time t for different turbulence realizations $\varepsilon(y,t)$, obtaining a time signal for the backscattered electric field $V(t)$. Given that the reflectometer signal is proportional to the backscattered electric field into the antenna, $V(t)$ can be taken as the hetereodyne signal $I(t) + iQ(t)$ and can be analysed as in the experiment. The applicability of the PO relies also on the good localization of the scattering process at the cutoff, this will be discussed in Sec. 4.2.

2.2. Extensions to the model

In order to apply PO to Doppler reflectometry consistently, the restriction on the turbulence level imposed by the Kirchhoff approximation has to be carefully considered. It has to be checked whether Eq. 1 is still valid in the range of parameters of interest.

The Kirchhoff approximation assumes the corrugation to be locally flat, neglecting the curvature of ε. Rodriguez [30] includes the curvature and gives a more general expression for the scattered electric field. For our specific case this corrections provides the extended model:

$$V = \cos\theta\int \mathrm{d}y \, \exp\left(-\frac{y^2\cos^2\theta}{w^2} + i2k_0 y\sin\theta\right)\exp\left(-i2k_0\varepsilon\cos\theta\right)\exp(-\varepsilon'\tan\theta)$$
$$\times\exp\left(-\frac{i(1+\tan^2\theta)\varepsilon''}{2k_0\cos\theta} - \frac{(\varepsilon'\tan\theta)^2}{2}\right)\left[\int \mathrm{d}y \, \exp\left(-\frac{y^2}{w^2}\right)\right]^{-1}. \tag{2}$$

Notice that while the first two exponentials appear also in the original model and the third one can be reduced to the term $\varepsilon'\sin\theta - \cos\theta$, the last exponential includes further

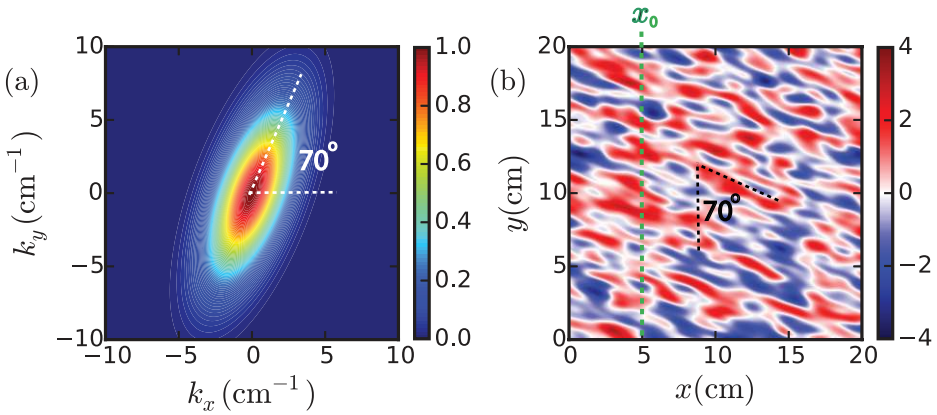

Figure 2. (a) 2D wavenumber spectrum $h_{2\mathrm{D}}(k_x, k_y)$ and (b) a sample of the turbulence field $\delta n(x, y)$. Elongation and tilting of the spectrum and turbulence structures can be observed.

correction considering the curvature through $\varepsilon'' = \mathrm{d}^2\varepsilon/\mathrm{d}y^2$. See appendix A for more details on the derivation. In Sec. 3.1 results from Eq. 1 and 2 are compared in order to establish the validity range of PO.

2.3. Synthetic turbulence

From theory [34] and simulations [35] the turbulence is expected to have a wavenumber spectrum characterized by a decay of the spectral intensity with k. Furthermore due to the different processes in the plasma, elongation and tilting of the turbulence structures are also anticipated [36]. Therefore for the modelling purposes of this paper it is reasonable to take a 2D Gaussian, elongated and tilted wavenumber spectrum:

$$h_{2\mathrm{D}}(k_x, k_y) = \frac{\ell_{\min}\ell_{\max}}{8\pi} \exp\left[-\frac{(k_x\cos\beta + k_y\sin\beta)^2\ell_{\min}^2 + (k_x\sin\beta - k_y\cos\beta)^2\ell_{\max}^2}{8}\right], \quad (3)$$

where β is the tilt angle of the spectrum respect to the x-axis, and $\ell_{\max}$ and $\ell_{\min}$ define the spectral minor and mayor spectral widths, respectively. Apart of including elongation and tilting the Gaussian shape provides well define statistical properties. This type of turbulence has been studied already in [37]. In this paper we use the $\ell_{\max} = 1.40$ cm, $\ell_{\min} = 0.51$ cm and $\beta = 70°$. The contour plots of $h_{2\mathrm{D}}$ are shown in Fig. 2a, where the elongation and the tilting can be recognized.

The turbulence field, $\delta n(x, y)$, is computed by 2D fast Fourier transform of $h_{2\mathrm{D}}$ after including random phases, a sample contour plot of the turbulence field is shown in Fig. 2b, where random, elongated and tilted structures can be observed. The obtained turbulence structures are predominantly elongated and tilted by 70° with respect to the y-axis. The correlation lengths along the major and minor axes are $\ell_{\max}$ and $\ell_{\min}$, respectively.

The physical optics considers the turbulence only at the cut-off layer, corresponding to a vertical slice of the turbulence field $\delta n(x_0, y)$. A sample of it is plotted in Fig. 3a. Taking the turbulence at a fixed x is equivalent to a delta Dirac filter in x-space, which

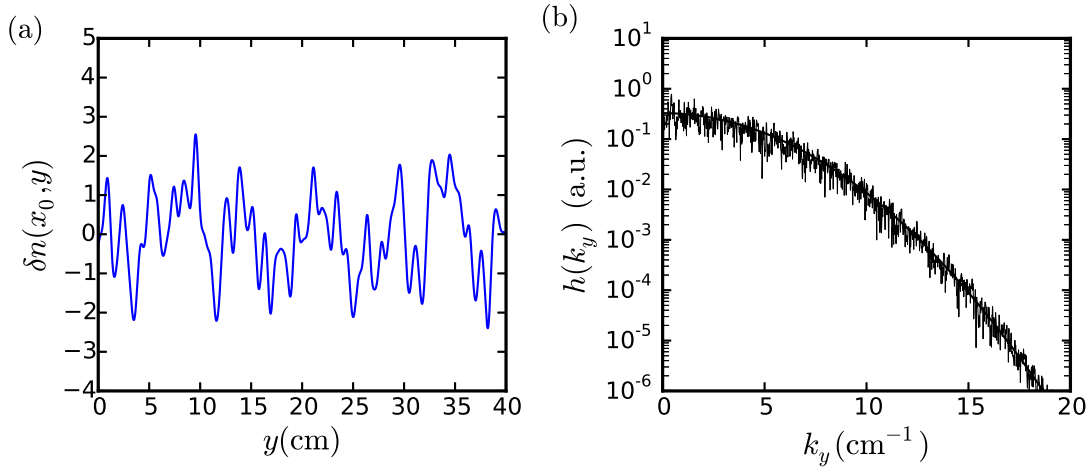

Figure 3. (a) Sample of the turbulence layer $\delta n(x_0, y)$ which is used as input for PO and (b) the corresponding perpendicular wavenumber spectrum $h(k_y)$, the thicker line depicts the input spectrum from Eq. 4.

requires the integration in the complete k_x-space. Integrating $h_{2\mathrm{D}}$ along k_x provides the spectrum of $\delta n(x_0, y)$ and equivalently the $k_\perp$-spectrum:

$$h(k_y) = \int_{-\infty}^{\infty} \mathrm{d}k_x h_{2\mathrm{D}}(k_x, k_y) = \frac{\ell_y}{\sqrt{8\pi}} \exp(-\ell_y^2 k_y^2/8). \tag{4}$$

ℓ_y is the perpendicular correlation length related to the 2D spectrum widths and tilting by

$$\ell_y = \frac{\ell_{\min}\ell_{\max}}{\sqrt{\ell_{\min}^2 \cos^2\beta + \ell_{\max}^2 \sin^2\beta}}. \tag{5}$$

In Fig. 3b the $k_\perp$-spectrum computed from $\delta n(x_0, y)$ is plotted, the thicker line depicts the input $h(k_y)$ from Eq. 4. For the parameter of this paper the perpendicular correlation length is $\ell_y = 0.54$ cm.

2.4. Numerical implementation

The integral in Eq. 2 is numerically computed (midpoint rule) over the interval $(-7w, 7w)$, ε is chosen to be proportional to the density turbulence δn at the cut-off which is shown in Fig. 3a, thus $\varepsilon(y) = \sigma\, \delta n(x_0, y)$. The field δn is normalized to have a standard deviation of 1, so that the turbulence level is given by the parameter $\sigma = \varepsilon_{\mathrm{rms}}$. Note that σ has the unit of a length.

Here in Sec. 2, we do a broad σ scan in order to study its role in the power response. Later on, in Sec. 4 when PO and 2D full wave simulations are compare, σ is related to the density and magnetic field profiles taking into account the polarization.

The time dependence is included by assuming the turbulence to be frozen and to move along the surface in the y-direction, $\delta n(x_0, y - u_\perp t)$. This is numerically achieved

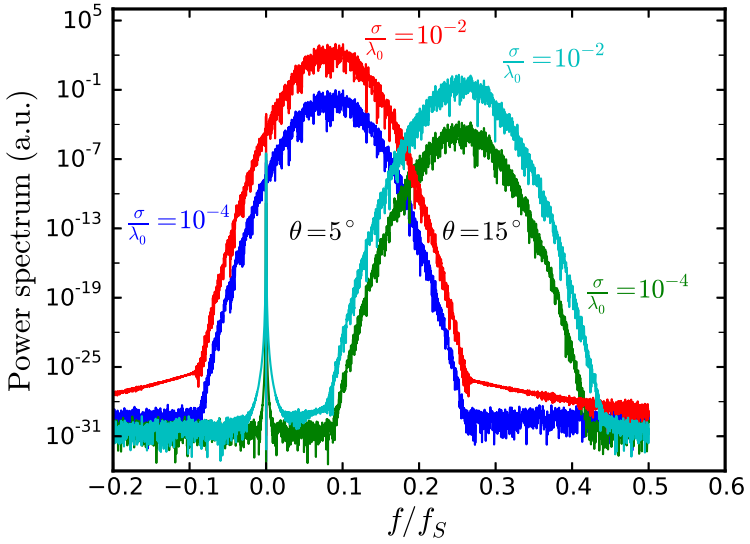

Figure 4. Power spectra of V simulated with PO for two angles of incidence θ and two turbulence levels σ. The position of the obtained Doppler peak depends on the angle of incidence and its intensity depends on the turbulence level.

by displacing the turbulence matrix n_d grid points between consecutive time steps, thus the perpendicular velocity of the turbulence is

$$u_\perp = \frac{n_d\,\Delta y}{\Delta t}, \tag{6}$$

with Δy the spatial resolution of the grid and Δt the time step. Note that Δt defines the sampling frequency $f_S = \Delta t^{-1}$.

2.5. Doppler reflectometer power response and $k_\perp$-spectrum measurement

The response of the Doppler reflectometer is now studied using PO. The complex signal $V(t)$ is computed for two incidence angles θ and two turbulence levels σ, with $w = 1.66$ cm and $\lambda_0 = 0.318$ cm corresponding to a probing frequency $f_0 = c/\lambda_0 = 94.4$ GHz. Fig. 4 shows the power spectra of the signal, where the x-axis corresponds to the frequency f normalized to the probing frequency f_S. There Doppler shifted peaks can be observed, that contain information on the backscattering with the turbulence at $k_\perp$ fulfilling the Bragg's condition

$$k_B = 2k_0 \sin\theta. \tag{7}$$

The area beneath the Doppler peak provides the backscattered power P, and its frequency shift f_D from 0 gives the perpendicular velocity $u_\perp = 2\pi f_D/k_B$.

For fixed θ, the Doppler peak intensity increases as the backscattered power increases with the turbulence level σ. The frequency shift f_D increases with θ as expected from Eq. 7. For a fixed σ, the Doppler peak intensity decreases with θ because of the smaller spectral density at larger k, Eq. 4.

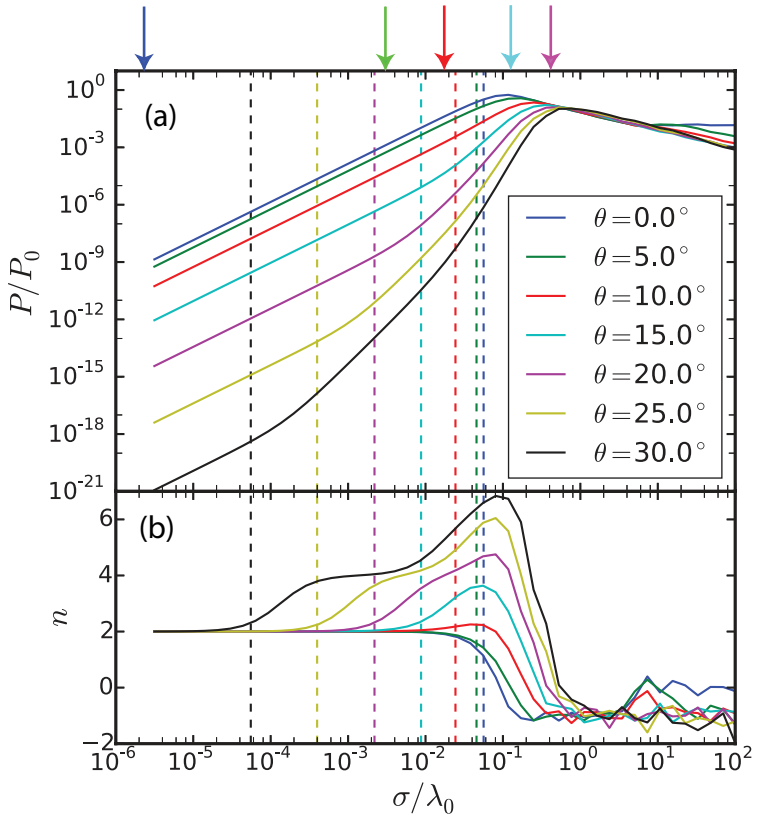

Figure 5. (a) Backscattered power P/P_0 and (b) scaling exponent n as a function of σ/λ_0. At small σ the response of the diagnostic is linear with σ^2. The critical turbulence level σ_c/λ_0 at which the response becomes non-linear is computed with Eq. 18, and is indicated for each angle with dashed lines.

In order to study the linear and non-linear response of the reflectometer, a scan in both σ and θ was performed. Fig. 5a depicts the backscattered power P as a function of the turbulence level σ (solid lines), the colours represent different θ values. σ is normalized with the characteristic length λ_0. Given the normalization of V in Eq. 2, the obtained power is normalized to the input power of the beam P_0.

It can be observed for small σ, that the power increases proportionally to σ^2 for all θ values. This is the the so called *linear regime*, where the power of the signal follows

$$P \propto \sigma^2 h^2(k_B). \tag{8}$$

With increasing σ the power reaches a maximum and then decreases with σ. In this *saturation regime* non-linear physical phenomena such as multiple and non-coherent scattering take place, which explains the decrease of the power despite a turbulence level increase.

The transition between the regimes is not always clear and appears to depend on θ. For small angles the transition from linear to saturation is immediate ($\theta = 0°$ blue line at $\sigma/\lambda_0 \approx 10^{-1}$). However, for larger θ there is an intermediate *non-linear regime* in which the power increases with σ faster than in the linear regime. Furthermore the location and extension of this regime depends on θ, for larger angles it starts at smaller σ and ends at larger σ.

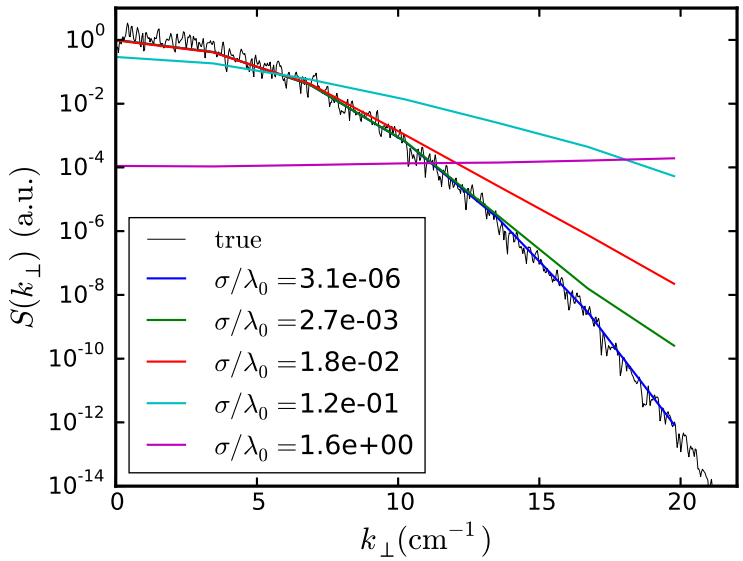

Figure 6. Input $k_\perp$-spectrum (black) and measured $k_\perp$-spectra with PO at different σ. A good agreement with the input spectrum is found for small σ (blue line) due to the linear response. For larger σ the spectral power is overestimated (green and red line) for large $k_\perp$ due to the enhanced power response. For the largest σ value (magenta line), the obtained spectrum is flat due to saturation.

This transition can be better analysed by considering the local scaling exponent n defined as $P \sim \sigma^n$, it is computed from the simulated data series as $n_i = \ln(P_{i+1}/P_i)/\ln(\sigma_{i+1}/\sigma_i)$. Fig. 5b shows n as a function of σ/λ_0 for the different values of θ from Fig. 5a. It confirms that for low turbulence level the response is linear since $n = 2$ is in agreement with Eq. 8. A transition to a *enhanced power response* non-linear regime before saturation is observed, which is characterized by an increase of n. The vertical dashed lines indicate analytic calculations of the transition points (see Sec. 3.2). Moreover for large angle, e.g. $\theta = 30°$, there is a σ range where $n \approx 4$, which indicates the existence of high order regimes with an enhanced power response. The saturation regime is observed when n decreases with σ.

The $k_\perp$-spectrum is reconstructed in Fig. 6 by plotting the backscattered power P as a function of k_B. The different colours represent various σ values, which are also marked by the vertical arrows at the top of Fig. 5a. The black line depicts the true $k_\perp$-spectrum computed from the turbulence field δn and corresponding to $h^2(k_y)$ from Eq. 4. Since the input turbulence is proportional to σ, all spectra have been normalized to σ^2 in order to compare the different cases with the input spectrum. For a small turbulence level (blue line) P gives a good measurement of the $k_\perp$-spectrum, as is expected in the linear regime, Eq. 8. When σ increases, the already discussed non-linear response flattens progressively the measured $k_\perp$-spectrum, until a flat spectrum is obtained in the saturation regime (magenta line).

The flattening of the perpendicular wavenumber spectrum has been observed in simulations and experiments [10, 18]. The common explanation states that the signal at small $k_\perp$ is saturated because of the higher amplitude of the turbulence while the signal

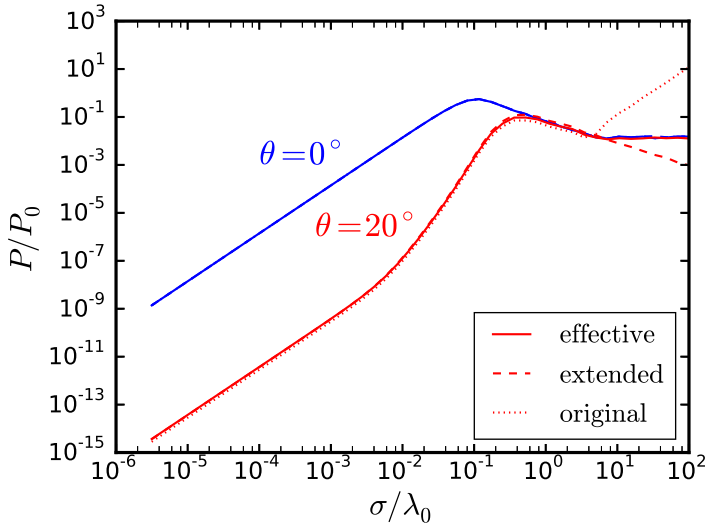

Figure 7. Backscattered power P/P_0 as a function of the turbulence level σ/λ_0. Extended (dashed), original (dotted) and reduced (solid) models are compared at normal and oblique incidence. All three models agree in the σ range of interest

at large $k_\perp$ is still linear. The results shown here contradict this explanation; the signal at large $k_\perp$ (large θ) is enhanced by the non-linear response ($n > 2$) and overestimates the spectral density, while the signal at small $k_\perp$ can still be linear and give an accurate measurement of the spectrum as shown in Fig. 6 (green line).

3. Advanced interpretation of the physical optics model

In order to assess the suitability of PO as an accurate and meaningful modelling tool, it is important to study the range of validity of PO regarding σ and to understand the role of each term in Eq. 2. This will allow to identify simplifications of Eq. 2, leading to a better understanding of the physical processes behind.

3.1. Effective physical optics model

We compute P as a function of σ for the extended model Eq. 2, the original model Eq. 1 and the *effective model* given by:

$$V = \cos\theta \int \mathrm{d}y \, \exp\left(-\frac{y^2\cos^2\theta}{w^2} + i2k_0 y \sin\theta\right) \exp(-2ik_0\varepsilon\cos\theta)$$
$$\times \left[\int \mathrm{d}y \, \exp\left(-\frac{y^2}{w^2}\right)\right]^{-1}. \qquad (9)$$

It corresponds to the Rodriguez's lowest order expression, which considers only basic scattering physics and no detailed interaction of the rough surface scattering problem (see appendix A for more details). The name given here is well justified later. The results for $\theta = 0°$ (blue) and $\theta = 22.7°$ (red) are shown in Fig. 7.

All the models agree for perpendicular incidence, this can be seen in Eq. 2 where the first order term and the second part of the second order term disappear for $\theta = 0°$. For oblique incidence, all the curves agree in the linear, non-linear and early saturation range. For the largest turbulence levels the original model diverges. The effective model saturates and the extended model decreases with the turbulence level.

We can conclude that, although the extended model treats more rigorously the problem of the scattering from a rough surface, the original and effective models are good enough in the σ range where we want to study the DR response. Hence the effects discussed in this paper occur in a parameter range where the PO model obtained with the Kirchhoff approximation remains valid. Furthermore the effective model of Eq. 9 is more suitable for analytic calculations as it is shown in the next section. The fact that the effective model is able to describe the power response, suggests that general scattering physics is relevant here, and not the specific rough surface scattering.

3.2. Perturbative expansion

The effective PO model, neglecting from now normalization terms, can be written as follows:

$$V = \int \mathrm{d}y \, \exp\left(-\frac{y^2\cos^2\theta}{w^2} + i2k_0 y\sin\theta\right)\exp(-i2k_0\varepsilon\cos\theta), \tag{10}$$

where the first exponential corresponds to a filter in k-space centred at k_B and with a spectral resolution given by $\Delta k = \sqrt{2}/w$. The filter f in real space and its Fourier transform (denoted by a hat) are respectively:

$$\begin{aligned} f(y) &= \exp\left(-\frac{(\Delta k)^2 y^2\cos^2\theta}{2} + iyk_B\right), \\ \hat{f}(k) &= \exp\left(-\frac{(k-k_B)^2}{2(\Delta k)^2}\right). \end{aligned} \tag{11}$$

The second exponential in Eq. 10 can be Taylor expanded obtaining

$$V = \int \mathrm{d}y f \exp(-i2k_0\varepsilon\cos\theta) \approx \int \mathrm{d}y \, f(1 - i2k_0\varepsilon\cos\theta - 2k_0^2\varepsilon^2\cos^2\theta + ...),$$

where the different order contributions can be separated obtaining the signal as a series of contributions,

$$V = \underbrace{\int \mathrm{d}y \, f}_{V_0} + \underbrace{(-i2)k_0\cos\theta\int \mathrm{d}y \, f\varepsilon}_{V_1} + \underbrace{(-2)k_0^2\cos^2\theta\int \mathrm{d}y \, f\varepsilon^2}_{V_2} + ... \tag{12}$$

The first term V_0 corresponds to the specular reflection which here is constant and typically excluded in Doppler Reflectometry data analysis.

The last equation can be regarded as an expansion in the parameter $\sigma = \varepsilon_{\mathrm{rms}}$ (turbulence level). If σ is small, the series can be cut at first order, then the magnitude of the reflectometer signal is proportional to the turbulence level Eq. 8 (linear regime). On the other hand, if σ is large, all other higher order terms in addition to V_1 play an important role and the reflectometer signal saturates.

For intermediate σ, the second order term V_2 can be important while all other high order terms are not. In this case the reflectometer signal is proportional to the square of the turbulence level σ^2 (*quadratic regime*), thus the power increases with the turbulence level faster than in the linear regime, with $n = 4$. There is a critical σ_c at which the transition from linear to quadratic regime takes place. It can also be considered the upper limit of the linear regime, which has been observed to move to lower turbulence levels with θ (Fig. 5) and with the correlation length of the turbulence (extra scans not shown here).

In order to calculate σ_c we estimate the magnitude of the different contributions in Eq. 12. The first order term is

$$V_1(t) = -i2k_0 \cos\theta \int \mathrm{d}y\, f(y)\varepsilon(y - u_\perp t), \tag{13}$$

The backscattered power can be computed from the Fourier transform of the signal. Due to the assumed linear dispersion relation $\omega = u_\perp k$, the Fourier transform can be computed in terms of k. Notice that $V_1(t)$ can be regarded as a convolution of $f(y)$ and $\varepsilon(y)$, therefore the Fourier transform is calculated using the convolution theorem

$$\hat{V}_1(k) = -i2k_0 \cos\theta \hat{f}(k)\hat{\varepsilon}(k) = -i2k_0 \cos\theta\sigma \hat{f}(k)h(k).$$

In the last expression the spectrum of ε is given by the $k_\perp$-spectrum and the turbulence level $\hat{\varepsilon}(k) = \sigma h(k)$. Notice that this first order term is linear in σ (turbulence level) and corresponds to the true $k_\perp$-spectrum filtered by $\hat{f}(k)$, this is in agreement with the linear response expected for a Doppler reflectometer.

The magnitude of $|\hat{V}_1|$ can be estimated taking into account that $\hat{f}$ gives contributions coming mostly from k_B,

$$|\hat{V}_1| \sim 2k_0 \cos\theta\sigma h(k_B), \tag{14}$$

which is reflected in the description of the linear regime in Eq. 8.

The second order term is

$$V_2(t) = -2k_0^2 \cos^2\theta \int \mathrm{d}y\, f(y)\varepsilon^2(y - u_\perp t),$$

following the same procedure done for the first order term, the Fourier transform is obtained,

$$\hat{V}_2(k) = -2k_0^2 \cos^2\theta \hat{f}(k)\hat{\varepsilon^2}(k) = -2k_0^2 \cos^2\theta \hat{f}(k)(\hat{\varepsilon} * \hat{\varepsilon})(k).$$

here we used the convolution $(*)$ theorem. The order of magnitude of this term can be estimated as

$$|\hat{V}_2| \sim 2k_0^2 \cos^2\theta\sigma^2 (h * h)(k_B). \tag{15}$$

Note that the second order term is quadratic in σ and involves the convolution:

$$(h * h)(k_B) = \int_{-\infty}^{\infty} \mathrm{d}k_1\, h(k_1)h(k_B - k_1). \tag{16}$$

The linear regime is characterized by a single scattering at k_B, Eq. 14, as it is shown schematically in the the $k_\perp$-spectrum in Fig. 8a. The black arrow represents the single

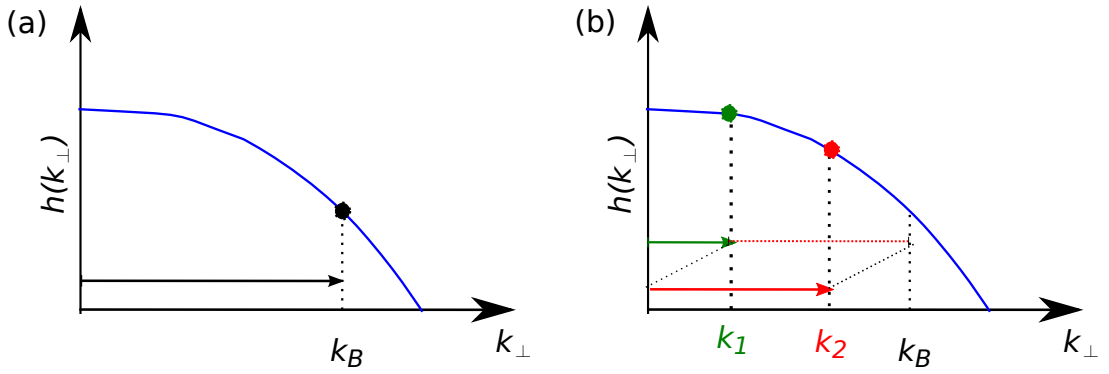

Figure 8. Schematic of (a) single and (b) double scattering processes represented on top of the $k_\perp$-spectrum. In (a) a single scattering event at k_B (black arrow) indicates contribution only from $h(k_B)$, while in (b) two scattering events with k_1 and k_2 (green and red arrows) give other other contributions.

scattering event, giving a contribution $h(k_B)$ only. Moreover according to Eq. 16, the quadratic regime is characterized by a double scattering event at k_1 and $k_2(= k_B - k_1)$ represented in Fig. 8b by green and red arrows, respectively. Contributions different from $h(k_B)$ are also indicated. Although the Bragg's condition is still fulfilled for the entire process $k_1 + k_2 = k_B$, the integration over k_1 implies the contribution of turbulence with multiple k_1 and k_2 to the reflectometer signal, thereby k-selectivity is impaired.

This effect can be extrapolated to higher order regimes, where multiple scattering events $k_1, k_2, k_3, \ldots$ give contributions from the entire wavenumber spectrum, independently of k_B and the incidence angle θ. This explains the flat spectra observed in the saturation regime.

The critical turbulence level σ_c is found by equating the first and second order terms, Eq. 14 and 15, respectively;

$$\begin{aligned} &|\hat{V}_1| = |\hat{V}_2|, \\ &2k_0 \cos\theta h(k_B)\sigma_c = 2k_0^2 \cos^2\theta \sigma_c^2 (h * h)(k_B), \\ &\frac{\sigma_c}{\lambda_0} = \frac{1}{2\pi \cos\theta} \frac{h(k_B)}{(h * h)(k_B)}. \end{aligned} \tag{17}$$

For the Gaussian $k_\perp$-spectrum under study (Eq. 4) this expression gives:

$$\frac{\sigma_c}{\lambda_0} = \frac{1}{2\pi \cos\theta\sqrt{2}} \exp\left(-\frac{\ell_y^2 k_B^2}{16}\right) = \frac{1}{2\pi \cos\theta\sqrt{2}} \exp\left(-\frac{\ell_y^2 k_0^2 \sin^2\theta}{4}\right). \tag{18}$$

This equation predicts a decrease of σ_c with θ and ℓ_y. In Fig. 5 σ_c is plotted as dashed lines together with the simulated data. A good match to the linear - non-linear transition is achieved.

In principle there are infinite regimes in which the reflectometer signal scales with σ^n but the range in which they appear is limited. For large σ, if the argument of the second exponential in Eq. 10 is larger than 1, all terms contribute and the series in Eq. 12 cannot be truncated any more, in this case saturation is reached. The turbulence

level for saturation σ_s can be roughly estimated from the magnitude of the term in the exponential

$$| - i2k_0 \cos\theta\varepsilon| \sim 2k_0 \cos\theta\sigma_s = 1,$$
$$\frac{\sigma_s}{\lambda_0} = \frac{1}{4\pi\cos\theta}. \tag{19}$$

Note that for normal incidence $\sigma_c \approx \sigma_s$, thus in this case there is a direct transition from the linear to the saturation regime as observed in Fig. 5a, while for oblique incidence transitions to higher order regimes occur in between σ_c and σ_s.

Equations 17 and 19 were derived without any assumption on the $k_\perp$-spectrum, therefore they are valid for any spectral shape. The exact occurrence of the enhanced power response regimes depends on the specific spectral shape. However if $h(k)$ decreases with k (as expected in real turbulence) a behaviour similar to the Gaussian case is obtained. For a plain $k_\perp$-spectrum ($\ell_y \to 0$ in Eq. 18) $\sigma_c \approx \sigma_s$ is obtained for every angle leaving no room for an enhanced power response, thus a direct transition from linear to saturation is obtained like in the normal incidence case. This case has been already observed with 2DFW codes in references [17, 25], where either a completely or locally (around k_B) flat $k_\perp$-spectrum was used and no enhanced power response was reported.

4. 2D full wave simulations

In order to study the existence of enhanced power response regimes in Doppler reflectometry, the power response is studied in detail using 2D full wave simulations. This modelling provides a complete description of the interaction between the microwave and the plasma, therefore these studies apply to the real response of a Doppler reflectometer. 2DFW simulations are performed using the code presented in [17]. Moreover the suitability of the PO model to describe the real power response is assessed later by comparing the results from the two modellings techniques for the same conditions.

Ordinary(O) and extraordinary(X) mode 2DFW simulations with probing frequencies $f_0 = 60.2$ and 94.4 GHz were performed, respectively. The background density profile is linear $n_0 = n_c(x/L)$ and the cut-off is located at $L = 5$ cm from the plasma boundary with a density $n_c = 4.5 \cdot 10^{19}$ m^{-3}. A uniform magnetic field with a strength of 2 T is applied. The beam waist is $w = 2.35$ and 1.66 cm for O- and X-mode, respectively. The turbulence field $\delta n(x, y)$ is normalized and added to the background density. The normalization is chosen to set the required turbulence level given by $\delta n_{\rm rms}/n_c$. Four values of θ are used such that the obtained $k_\perp$ in between 2 and 12 cm^{-1} is experimentally meaningful. These parameters correspond to typical ASDEX Upgrade conditions.

An example of the electric field contour plots for O-mode are depicted in Fig. 9. The angle of incidence is 17.7° with respect to the normal of the plasma density isolines.

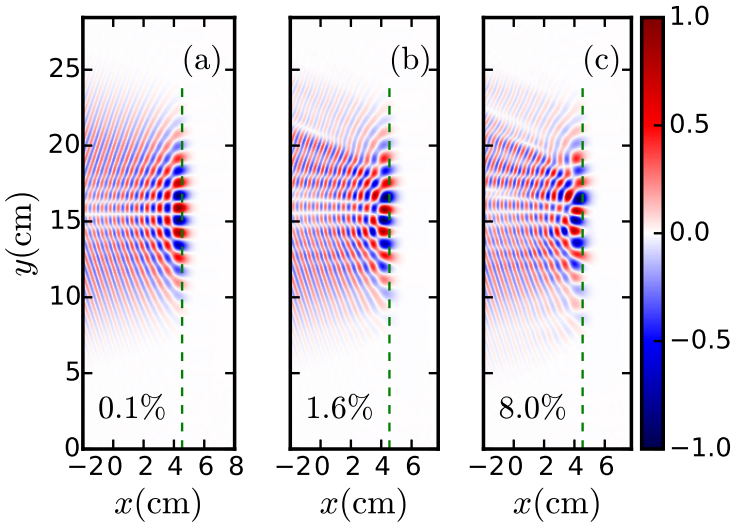

Figure 9. Electric field contour plots for O-mode with an incidence angle $\theta = 17.7°$ and different turbulence level $\delta n/n_c = 0.1\%$ (a), 1.6% (b) and 8.0%. The nominal cutoff is indicated by a dashed line.

The different plots correspond to various $\delta n_{rms}/n_c$. For low turbulence level Fig. 9a the beam propagation is barely affected by the turbulence. For higher turbulence level Fig. 9b and c an interaction with the turbulence is noticeable and the reflected beam is perturbed.

4.1. Power response

The points in Fig. 10a and b show the backscattered power P computed from 2DFW as a function of the turbulence level $\delta n_{\rm rms}/n_c$ for O- and X-mode, respectively. The solid lines depict the results from PO which are discussed in the following sections. For low turbulence level ($\sim$0.1%) a linear response can be observed specially for the O-mode and small θ X-mode. For larger turbulence level ($\sim$1.0%) a faster growth of the power with $\delta n_{rms}/n_c$ is evident for large θ and specially X-mode, this indicates an enhanced power response. For the largest turbulence level ($\sim$8.0%) a saturation of the power is observed. In order to study the linearity of the response, the scaling exponent n is computed and plotted in Fig. 10c and d for O- and X-mode, respectively. The occurrence of $n > 2$ for turbulence levels in between the linear and non-linear saturation regime confirms the existence of the enhanced power response regimes in DR.

Note that for a fixed θ, the X-mode power response becomes non-linear at a lower turbulence level compared to O-mode, indicating that the latter is better suited for Doppler reflectometry. This is relevant for some application e.g. for radial correlation Doppler reflectometry [38], where the comparison is performed at the same angle of incidence. Nevertheless the role of the probed k_B in the linearity of the response will be discussed later.

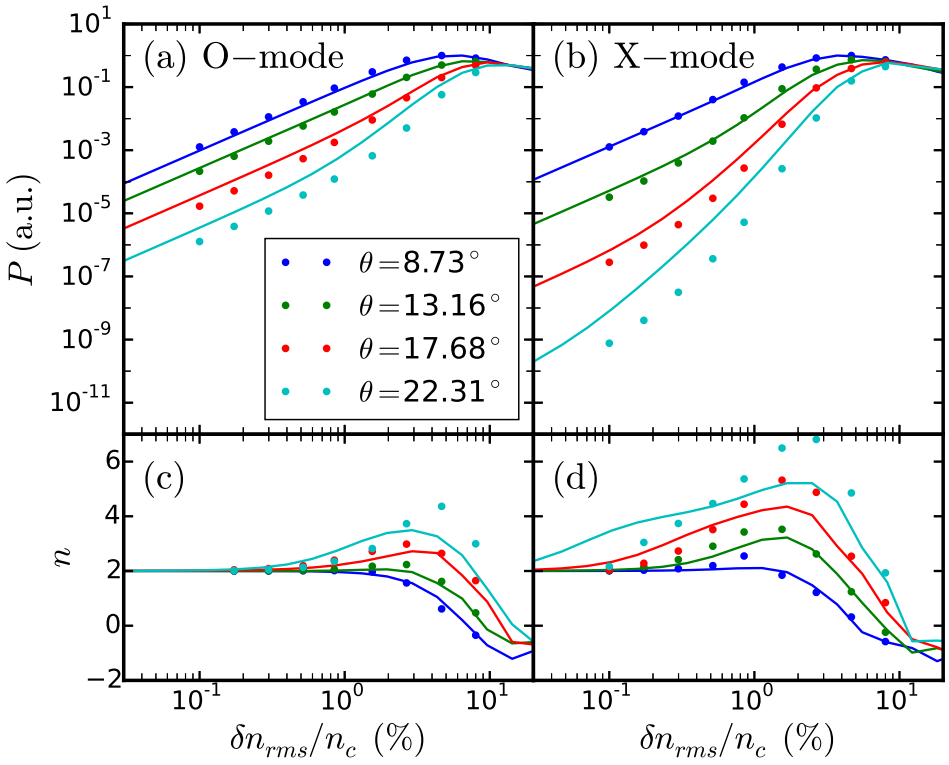

Figure 10. Power P for (a)O and (b)X-mode, and scaling exponent n for (c)O- and (d)X-mode as a function of the turbulence level for different angles. 2DFW data are plotted with points and PO results with solid lines.

The 2DFW results are in qualitative agreement with those obtained with PO. Hence the same interpretation in terms of multiple scattering processes seems to be valid in general for DR, particularly the enhanced regimes can be explained by double and triple scattering events.

4.2. On the applicability of the physical optics model

In reality the interaction of the microwave beam with the plasma is a complex process. Apart from the backscattering at the cutoff layer, forward and backscattering along the incident and reflected beams are possible and may contribute to the reflectometer signal. Nevertheless due to the minimization of the refractive index at the cutoff, the main contribution to the DR signal is expected to be the backscattering well localized in this region [7]. The last argument justifies the use of PO as a modelling tool for DR, given that all plasma-wave interactions away from the cutoff are neglected.

In order to apply consistently PO the localization of the scattering has to be assessed, at least for the case under study. This can be done using the weighting function, which indicates the localization of the scattering in the linear regime [39, 40]. The absolute value of the weighting function $|W|$ was computed from 2DFW data, it corresponds to the squared electric field without turbulence averaged within a microwave

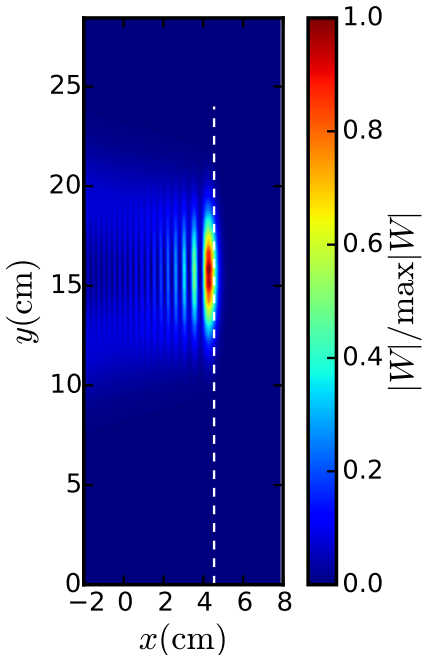

Figure 11. Absolute value of the weighting function computed from 2DFW data for O-mode and $\theta = 19.7°$, normalized to its maximum value in the simulated domain. The strongest contribution can be observed at the cutoff, which is indicated with a dashed line.The good localization of the interaction justifies the PO application.

period. In Fig. 11 an example weighting function is shown, which corresponds to the O-mode case at $\theta = 17.7°$. The strongest contribution can be observed at the cutoff (there is a slight displacement which is discussed in the Appendix B), whereas weaker contributions appear in other regions. The dominance of the cutoff contribution justifies the application of PO for this case. It is important to remark that although the weaker contributions away from the cutoff are not relevant for the power response, they may be important for radial correlation length studies, where signal contributions of very low amplitude can still give strong correlations [41].

The weighting function argument is valid only in the linear regime. In the strong non-linear regime (saturation) the incoming beam is substantially affected by the turbulence before it reaches the cutoff, as can be seen in Fig. 9c. This effect is not included in the PO model, where the beam is always smooth (however a perturbation of the beam could be included in Eq. 2), hence the PO is not expected to be a good approximation in such regime. Nevertheless for moderate turbulence level like in Fig. 9b, where the enhanced power response appears, this effect is small and the PO modelling is a reasonable approximation to DR.

4.3. Comparison with physical optics results

In order to compare the physical optics and 2DFW, the density turbulence δn of 2DFW has to be translated into a corrugation ε for PO. This is done by considering the linear

(Born approximation) O-mode theory presented in [20], where the backscattered signal is proportional to

$$V_{\text{Born}} \propto \int_{\text{plasma}} \mathrm{d}\vec{r}\, \delta n(\vec{r}) E_0^2(\vec{r}). \tag{20}$$

E_0 is the electric field of the probing beam as if there was no density turbulence.

In the last expression and in the linear contribution (Eq. 13) of PO the turbulence is *weighted* by a function related to the beam and integrated over a certain domain, the weighting function is $E_0^2(\vec{r})$ and $f(y)$, respectively. In order to make Eq. 13 and 20 analogous $\varepsilon \propto \delta n$ is chosen, which means using the density turbulence δn as the corrugation in PO with a proper normalization.

Accordingly, we define a normalization factor N linking the turbulence level in PO and 2DFW,

$$\frac{\delta n_{\text{rms}}}{n_c} = N\sigma. \tag{21}$$

This normalization factor must account for the density gradient and magnetic field, as well as the polarization which are no included in PO.

It is possible to estimate N using the already developed non-linear conventional reflectometry theory from [20, 42]. For normal incidence, it predicts the critical turbulence level for transition to the non-linear regime as,

$$1 = \left(\frac{\delta n_{\text{rms}}}{n_c}\right)_s^2 \frac{G^2 (2\pi)^2 L^{\text{ref}} \ell_x}{\lambda_0^2} \ln\left(\frac{L^{\text{ref}}}{\ell_x}\right), \tag{22}$$

where L^{ref} is the gradient scale length of the refractive index, which depends on the polarization, and ℓ_x is the correlation length of the turbulence in the x-direction which for our case is 1.05 cm. In the last expression the polarization is also included in the enhancement factor G [43],

$$G = \begin{cases} 1 & \text{for O-mode} \\ \dfrac{(\omega_0^2 - 2\omega_p^2)(\omega_0^2 - \omega_c^2) + \omega_p^4}{(\omega_0^2 - \omega_p^2 - \omega_c^2)^2} & \text{for X-mode} \end{cases}, \tag{23}$$

with $\omega_0 = 2\pi f_0$, and $\omega_p = \sqrt{n_0 e^2/\epsilon_0 m}$ and $\omega_c = eB/m$ the electron plasma and cyclotron frequencies, respectively.

Since the critical turbulence level for normal incidence in PO is provided by Eq. 19, it can be compared with Eq. 22 in order to estimate N. Setting $(\delta n_{\text{rms}}/n_c)_s = N\sigma_s$ one obtains

$$N = \sqrt{\frac{4}{G^2 L^{\text{ref}} \ell_x \ln(L^{\text{ref}}/\ell_x)}}. \tag{24}$$

For O-mode the refractive index is linear in the plasma density, therefore L^{ref} corresponds to the density gradient scale length $(\nabla n_0/n_0)^{-1}$. It means $L^{\text{ref}} = L = 5$ cm for our linear density profile. For X-mode on the other hand, the magnetic field has to be taken into account. The refractive index was numerically computed and from

its gradient at the cut-off we obtain $L^{\mathrm{ref}} \approx 0.5L$. The enhancement factor for X-mode computed at the cut-off is $G \approx 4.9$.

The same f_0, w and θ as for 2DFW were used for PO simulations, furthermore a broad and fine scan of σ was performed. Note that the difference between O- and X-mode is included through the different f_0, w, G and L^{ref}. Using the normalization given in Eq. 21, the PO data are plotted with continuous lines together with 2DFW results (points) in Fig. 10. Here the qualitative agreement in terms of the occurrence of the different regimes is evident.

It is remarkable that the difference between O- and X-mode is reproduced by the PO only by the choice of f_0. According to PO, Eq. 17 indicates that the linearity depends mainly on k_B and the specific h. Therefore the large difference observed between both polarizations is mainly due to the intrinsically smaller k_B of the O-mode. Thus if O- and X-mode are compared at the same θ, O-mode response is expected to be much more linear, whereas this difference is not expected if they are compared at the same k_B. However the normalization factor N from Eq. 24 introduces a difference in the linearity of the response between both polarizations.

The agreement of PO and 2DFW for O- and X-mode at $\theta = 8.73°$ (close to normal incidence), suggests that the normalization factor N from Eq. 24 is appropriate, thus PO may be used for quantitative estimations in DR. However here only one scenario of ℓ_x, and density and magnetic field profiles has been studied. Further studies are require in order to validate this normalization factor, specially for the case of shallow density gradients where PO may fail [23] . Nevertheless the general character of Eq. 22 indicates that it might remain valid.

Although 2DFW and PO have a qualitatively similar behaviour there are some quantitative differences. In the pure linear regime at low turbulence level the two models do not agree, the decay of P with θ is slower for PO. The scaling exponent n has comparable values and seems to match better for small θ, while for large θ PO run first into non-linear regime. In the following sections those differences are studied and the possibility of a renormalization is discussed, seeking a better quantitative agreement between PO and 2DFW modelling. Nevertheless, it is remarkable that PO can reproduce indeed most of the features of the 2DFW power response.

4.4. Linear response

The 2DFW simulations are extended in order to study the linear response, more angles (including normal incidence) and lower turbulence level (0.01%) for X-mode are included. The $k_\perp$-spectra computed from the simulated data in linear regime are plotted with circles in Fig. 12a, the black line represents the input spectrum, Eq. 4. Although the reflectometer is operating in the linear regime, the reconstructed $k_\perp$-spectrum underestimates the true one for both O- and X-mode. Notice that the PO measurements do match the true $k_\perp$-spectrum because the linear response is reduced to the $k_\perp$-filter according to Eq. 14, the factor $\cos\theta$ gives a negligible corrections.

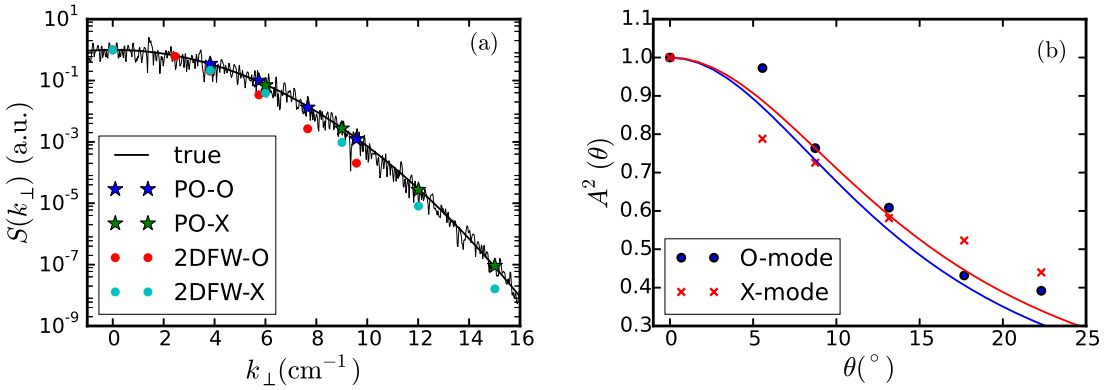

Figure 12. (a) $k_\perp$-spectra in the linear regime obtained with O-mode and X-mode from PO and 2DFW, the black line depicts the input one. 2DFW underestimates the true spectrum. (b) Ratio of the 2DFW power and the input spectral density, it gives the correction factor $A^2(\theta)$ necessary to recover the true $k_\perp$-spectrum

It is usually assumed that Doppler Reflectometry can provide a good measurement of the $k_\perp$-spectrum (Eq. 8), at least in the linear regime. However there is no reason to discard possible extra dependencies of the backscattered power on the parameters, e.g. on θ or k_B. Such dependencies have been already observed in 2DFW simulations [17, 18, 45], where a correction factor was necessary in order to recover the input spectrum. Results from linear theory also confirm that the so called *scattering efficiency* affects the backscattered power [44] and may introduce a factor depending on the angle of incidence.

The power measured by the reflectometer can be written

$$P_{\mathrm{2DFW}} = C \left(\frac{\delta n_{rms}}{n_c} \right)^2 A^2(\theta) h(k_B)^2, \tag{25}$$

where a correction factor $A(\theta)$ accounting for the scattering efficiency has been included, and C is a normalization constant of the power. $A^2(\theta)$ is computed by dividing P_{2DFW} by the true spectral intensity $h(k_B)^2$, the data are normalized to the normal incidence and plotted (points) as a function of θ in Fig. 12b. The proposed $A(\theta)$ to be explained next is depicted with solid lines. It is observed that the sensitivity of the reflectometer decreases with θ considerably, also similar behaviour for O- and X-mode is observed.

Although a detailed and consistent study of the scattering efficiency is needed, we derive and discuss in Appendix B the following formula which should be taken as a first approximation. Considering the k^{-1} dependency of the Green function for the Helmholtz operator in the relevant geometry, and calculating the k value at the scattering position, one can show that:

$$A(\theta) = \left[1 + \left(\frac{2\pi L^{\mathrm{eff}}}{\lambda_0} \right)^{2/3} \sin^2\theta \right]^{-1/2}. \tag{26}$$

L^{eff} is the gradient length of the refractive index, which for O-mode is L from the density profile, and for X-mode is approximately $0.5L$ for the given parameters.

Equation 26 is able to follow approximately the simulated data for O- and X-mode, see Fig. 12. Thus 2DFW $k_\perp$-spectra for the linear response can be corrected in order to get the true one.

4.5. Alternative normalization for the physical optics

The scattering efficiency can also be used to improve the quantitative agreement of PO with 2DFW. The power in PO can be renormalized using $A(\theta)$, obtaining an agreement of the measured $k_\perp$-spectrum of PO and 2DFW in the linear regime. However it has also been observed in [23], that renormalizing the PO turbulence level can also improve the agreement between the two models. Therefore including the scattering efficiency $A(\theta)$ in the normalization constant N from Eq. 24, could improve the match in the linear and non-linear regimes.

5. Discussion on application to experimental data analysis

Although these studies were performed in slab geometry and with a linear density profile, they could be applied in DR experimental data analysis. The scattering efficiency expression in Eq. 26 can be used to correct the measured $k_\perp$-spectrum when the reflectometer is operating in the linear regime. In the experiment θ can be extracted from $k_\perp = 2k_0 \sin\theta$ where $k_\perp$ is typically obtained using ray tracing, and the refractive index gradient length L^{ref} can be computed from the density and magnetic field profiles.

The linearity criterion for normal incidence [42] can be generalized to oblique incidence using the physical optics linearity criterion Eq. 17, obtaining

$$\left(\frac{\delta n_{\mathrm{rms}}}{n_c}\right)^2 \frac{G^2(2\pi)^2 L^{\mathrm{ref}} \ell_r}{\lambda_0^2} \ln\left(\frac{L^{\mathrm{ref}}}{\ell_r}\right) \left[\frac{\cos\theta}{2} \frac{(h * h)(2k_0 \sin\theta)}{h(2k_0 \sin\theta)}\right]^2 \ll 1, \quad (27)$$

where ℓ_r is the radial correlation length of the density turbulence. This may be a useful tool for DR, because it allows to evaluate whether the response is still linear considering θ. Its effect is relevant since it reduces considerably the range of linear operation specially for large θ.

The last expression requires previous knowledge on the $k_\perp$-spectrum and radial correlation length, however if a Gaussian spectrum is assume and an estimation of the correlation length ℓ is used, the previous condition can be easily evaluated as follows:

$$\left(\frac{\delta n_{\mathrm{rms}}}{n_c}\right)^2 \frac{G^2(2\pi)^2 L^{\mathrm{ref}} \ell}{\lambda_0^2} \ln\left(\frac{L^{\mathrm{ref}}}{\ell}\right) \left[\frac{\cos\theta}{\sqrt{2}} \exp\left(\frac{\ell^2 k_0^2 \sin^2\theta}{4}\right)\right]^2 \ll 1, \quad (28)$$

Finally PO can be used to calculate efficiently the response to a trial $h(k_\perp)$, which can be compared with the experimental $k_\perp$-spectrum. From the comparison a better trial $h(k_\perp)$ could be proposed and the same procedure repeated. After some iterations the true $k_\perp$-spectrum could be obtained self-consistently. The technical implementation and a proof of principle are out of the scope of this paper and left for future work.

6. Conclusions

The physical optics model has been used as an approximation to study the power response of Doppler reflectometry. The linear and non-linear saturation regimes already observed in the references [17, 19, 20] are recovered, however for oblique incidence, higher order regimes with an enhanced power response are observed. They are characterized by scaling exponents larger than 2, i.e. the backscattered power grows faster with the turbulence level than in the linear regime. This enhanced power response is found to be responsible for the flattening of the $k_\perp$-spectrum, which is over-estimated at large $k_\perp$.

After checking the range of applicability of physical optics, the different regimes have been studied analytically. A perturbative expansion of the backscattered signal in the turbulence level has been proposed. This expansion explains the different regimes as contributions from a multiple scattering process. Furthermore, an analytical expression for the critical turbulence level for linear response has been found.

Moreover, the power response of Doppler reflectometry has been studied by means of 2D full wave simulations for O- and X-mode. For this more realistic case, the enhanced power response regimes are also found in qualitative agreement with the physical optics results. The latter suggests that the interpretation proposed for physical optics, regarding the enhance power response regimes and the multiple scattering process, can be applied to the understanding of 2D full wave simulations, and therefore Doppler reflectometry in general.

It has also been observed that O-mode is better suited for Doppler reflectometry turbulence level measurements, since its response is linear over a wider range in turbulence levels compared with the X-mode for the same angle of incidence. This difference is mostly due to the intrinsic smaller $k_\perp$ values probed with O-mode. Nevertheless the specific conditions of the density profile and magnetic field can make O-mode globally more linear than the X-mode.

It is found that the 2D full wave simulations in the linear regime underestimate the $k_\perp$-spectrum due to the scattering efficiency. This effect is investigated and a simple formula to describe it has been proposed as a first approximation. Finally applications to Doppler reflectometry data analysis based on these results are discussed, in particular the linearity criterion from [42] has been extended to include measurements at oblique incidence and a formula to assess the linearity of the Doppler reflectometry measurements has been provided.

Acknowledgements

This work was supported by the European Commission within the framework of the Erasmus Mundus International Doctoral College in Fusion Science and Engineering (FUSION-DC). The views and opinions expressed here do not necessarily reflect those of the European Commission. This work was also performed within the framework of the Helmholtz Virtual Institute on Plasma Dynamical Processes and Turbulence Studies

using Advanced Microwave Diagnostics.

References

[1] Mazzucato E 1976 *Phys. Rev Lett.* **36** 792
[2] Surko C M and Slusher R E 1976 *Phys. Rev. Lett.* **37** 1747
[3] Hennequin P *et al* 2004 *Plasma Phys. Control. Fusion* **46** B121
[4] Senet A *et al* 1980 *Phys. Rev. Lett.* **45(6)** 445
[5] Brower D L *et al* 1987 *Nucl. Fusion* **27** 2055
[6] Hirsch M *et al* 1999. *Proc. 4th Int. Reflectometry Workshop (Cadarache, France)*
[7] Hirsch E, Holzhauer E, Baldzuhn J and Scott B 2001 *Plasma Phys. Control. Fusion* **43** 1641
[8] Hennequin P. *et al* 2006 *Nucl. Fusion* **46** S771
[9] Happel T. *et al* 2011 *Phys. Plasmas* **18** 102302
[10] Fernández-Marina F Estrada T and Blanco E 2014 *Nucl. Fusion* **54** 072001
[11] Vermare L *et al* 2011 *Phys. Plasmas* **18** 012306
[12] Schirmer J *et al* 2006 *Nucl. Fusion* **46** S780
[13] Estrada T. *et al* 2009 *Plasma Phys. Control. Fusion* **51** 124015
[14] Happel T *et al* 2016 *Plasma Phys. Control. Fusion* **56** 064004
[15] Conway G D *et al* 2011 *Phys. Rev. Lett.* **106** 065001
[16] Schirmer J *et al* 2007 *Plasma Phys. Control. Fusion* **49** 1019
[17] Blanco E and Estrada T 2008 *Plasma Phys. Control. Fusion* **50** 095011
[18] Lechte C *et al* 2007 *Proc. 8th Int. Reflectometry Workshop (St Petersburg, Rusia)*
[19] Gusakov E Z *et al* 2004 *Plasma Phys. Control. Fusion* **46** 1143
[20] Gusakov E Z *et al* 2005 *Plasma Phys. Control. Fusion* **47** 959
[21] Conway G D 1999 *Plasma Phys. Control. Fusion* **41** 65
[22] Conway G D 1997 *Plasma Phys. Control. Fusion* **39** 407
[23] Conway G D *et al* 2002 *Plasma Phys. Control. Fusion* **44** 451
[24] Blanco E and Estrada T 2013 *Plasma Phys. Control. Fusion* **55** 125006
[25] Da Silva F *et al* 2010 *IEEE Transactions on Plasma Science* **38(9)** 2144
[26] Beckmann P and Spizzichina A 1963 *The Scattering of Electromagnetic Waves from Rough Surfaces* (Oxford: Pergamon)
[27] Robinson I S 2004 *Measuring the Oceans: The Principles and Methods of Satellite Oceanography* (Chichester: Springer)
[28] Wang L and Qu J J 2009 *Front. Earth Sci. China* **3(2)** 237
[29] Röttger J 1980 *Radio Sci.* **15(2)** 259
[30] Rodriguez E 1989 *Radio Sci.* **24(5)** 681
[31] Rodriguez E 1991 *Radio Sci.* **26(1)** 121
[32] Lynch P J 1970 *J. Acoust. Soc. Am.* **47(3)** 804
[33] Ejiri E *et al* 2008 *Plasma Phys. Control. Fusion* **50** 065003
[34] Kolmogorov A N 1991 *R. Soc. Lond. A* **434** 15 (reprint)
[35] Liewer P C 1985 *Nucl. Fusion* **25** 543
[36] Fedorczak N *et al* 2013 *Plasma Phys. Control Fusion* **55** 124024
[37] Pinzón J R *et al* 2015 *Proc. 12th Int. Reflectometry Workshop (Jülich, Germany)*
[38] Pinzón J R *et al* 2016 *Proc. 43rd EPS Conf. on Plasma Physics (Leuven)* to be published
[39] Bulanin V and Yafanov M 2006 *Plasma Phys. Rep.* **32** 47
[40] Conway G D *et al* 2015 *Proc. 12th Int. Reflectometry Workshop (Jülich, Germany)*
[41] Gusakov E Z *et al* 2014 *Plasma Phys. Control. Fusion* **56** 025009
[42] Gusakov E Z *et al* 2002 *Plasma Phys. Control. Fusion* **44** 1565
[43] Gusakov E Z *et al* 2015 *Plasma Phys. Control. Fusion* **57** 075009
[44] Gusakov E Z and Tyintarev M A 1997 *Fusion Eng. Des.* **34-35** 501

[45] Blanco E, Estrada T and Holzhauer E 2007 *Proc. 8th Int. Reflectometry Workshop (St Petersburg, Rusia)*
[46] Weber H, Maj O and Poli E 2015 *EPJ Web of Conferences* **87** 01002
[47] Morse P M and Feshbach H 1953 *Methods of Theoretical Physics* Part I (New York: McGraw-Hill Book Company) p 811
[48] White R B and Chen F F 1974 *Plasma Phys.* **16** 565

Appendix A. Extension of the Physical Optics model

The Kirchhoff approximation [26] calculates the reflected electric field by a corrugated conducting surface assuming it locally flat, meaning this that the radius of curvature of the surface corrugation is much larger than the incident wavelength λ_0, Fig. A1a. This condition is not always granted, especially for large corrugations ε, Fig. A1b.

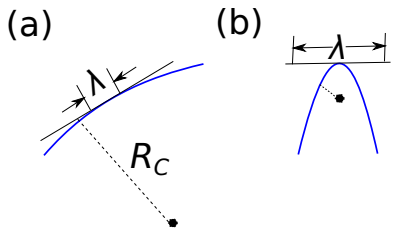

Figure A1. Wavelength compared with the curvature of the surface corrugation, for a large curvature radius R_C (a) the surface can be assumed locally flat and Kirchhoff approximation holds, but not for a small curvature radius as in (b).

The Kirchhoff approximation limits the applicability of the model to small fluctuation levels. Such limitation was overcome by Rodriguez [30]. Here we present his results and apply them to our particular case.

The back-scattered field in the far region is given by (Eq. 33 in [30])

$$V = \int \mathrm{d}y \, \exp(i2k_0 y \sin\theta) \exp(-ik_0 \varepsilon \cos\theta) F(y), \tag{A.1}$$

with $f(y)$ the following cumulant expansion (Eq. 21 in [30])

$$F(y) = -k_0 \cos\theta \exp(-ik_0 \varepsilon \cos\theta) \exp\left(\sum_1^\infty \frac{g^{(n)} \alpha^n}{n!} \right). \tag{A.2}$$

The series in the last exponential introduces a *momentum transfer perturbation expansion*, where α is a small parameter proportional to the ratio of momentum transfer in the y-direction to momentum transfer in the x-direction. The smallness of α allows to cut the series up to some order and to obtain a closed expression. The first two terms in the series are:

$$g^{(1)}\alpha = -\varepsilon' \tan\theta,$$

$$g^{(2)}\alpha^2 = -\frac{i}{k_0 \cos\theta}(1 + \tan^2\theta)\varepsilon'' - (\varepsilon' \tan\theta)^2.$$

Notice that the beam term $\exp(-\cos^2\theta y^2/w^2)$ can be included in Eq. A.1

To 0th order in α, the backscattered electric field is,

$$V = -k_0\cos\theta\int \mathrm{d}y\, \exp\left(-\frac{y^2\cos^2\theta}{w^2} + i2k_0 y\sin\theta\right)\exp(-2ik_0\varepsilon\cos\theta). \tag{A.3}$$

Including the normalization factor the last expression gives the effective model Eq. 9 discussed in Sec. 3.1.

To first order in α it is

$$V = -k_0\cos\theta\int \mathrm{d}y\, \exp\left(-\frac{y^2\cos^2\theta}{w^2} + i2k_0 y\sin\theta\right)\exp(-2ik_0\varepsilon\cos\theta)\exp(-\varepsilon'\tan\theta). \tag{A.4}$$

Notice that in the first order expression, Eq. A.4, the last term can be Taylor expanded, $\exp(-\varepsilon'\tan\theta) \approx 1 - \varepsilon'\tan\theta = -(\varepsilon'\sin\theta - \cos\theta)/\cos\theta$, recovering the original PO model [21].

To second order one obtains

$$V = -k_0\cos\theta\int \mathrm{d}y\, \exp\left(-\frac{y^2\cos^2\theta}{w^2} + i2k_0 y\sin\theta\right)\exp(-2ik_0\varepsilon\cos\theta)\exp(-\varepsilon'\tan\theta)$$
$$\times\exp\left(-\frac{i(1+\tan^2\theta)\varepsilon''}{2k_0\cos\theta} - \frac{(\varepsilon'\tan\theta)^2}{2}\right).$$

The second derivative ε'' contains the *curvature* of the corrugation, going beyond the Kirchhoff approximation.

The last expression can be normalized to the reflected electric field without turbulence for perpendicular incidence, instead of oblique as in [21]. This allows to compare the signal at different angles of incidence as it is done in the experiments, e.g. for perpendicular wave number spectra studies. Thus the extended model is

$$V = \cos\theta\int \mathrm{d}y\, \exp\left(-\frac{\cos^2\theta y^2}{w^2} + i2k_0 y\sin\theta\right)\exp\left(-i2k_0\varepsilon\cos\theta\right)\exp(-\varepsilon'\tan\theta)$$
$$\times\exp\left(-\frac{i(1+\tan^2\theta)\varepsilon''}{2k_0\cos\theta} - \frac{(\varepsilon'\tan\theta)^2}{2}\right)\left[\int \mathrm{d}y\, \exp\left(-\frac{y^2}{w^2}\right)\right]^{-1}, \tag{A.5}$$

Appendix B. Scattering efficiency

The effect of the scattering efficiency has been already observed in 2DFW simulations [17, 18, 45], however it is not yet well understood and predictions applicable to experimental data analysis are not available. Although a detailed and consistent study of the scattering efficiency is needed, we derive here a formula which should be understood as a first approximation. Nevertheless it recovers the trends of the presented simulations, and allows to understand the role of the basic parameters. A detailed validation of the proposed formula and a rigorous study of the scattering efficiency are left for future work.

The electric field E for O-mode propagation in cold plasma is described by,

$$(\nabla^2 + k^2)E = \left[\nabla^2 + k_0^2\left(1 - \frac{n_0}{n_c}\right)\right]E = k_0^2\frac{\delta n}{n_c}E \tag{B.1}$$

where $k^2 = k_0^2(1 - n_0/n_c)$ with $n_c = \epsilon_0 m\omega^2/e^2$ and n_0 the electron density without turbulence.

If $\delta n \ll n_c$, the Born approximation applies [46]. Thus the electric field can be written as $E = E_0 + E_1$, where E_0 is the electric field for the no-turbulence case and E_1 is the scattered field. Given that the fields satisfy $E_1 \ll E_0$, after replacing E in Eq. B.1 one finds,

$$(\nabla^2 + k^2)E_0 = 0, \tag{B.2}$$

$$(\nabla^2 + k^2)E_1 = k_0^2 \frac{\delta n}{n_c} E_0 \tag{B.3}$$

Note that E_0 fulfils the homogeneous Helmholtz equation, while E_1 satisfies the inhomogeneous Helmholtz equation with a source term (right hand side) proportional to $\delta n E_0$. It means that the scattering is produced by the interaction of the unperturbed field with the density turbulence.

The scattered field E_1 can be computed using the Green function G of the 2D Helmholtz operator using,

$$E_1 = k_0^2 \int \mathrm{d}x\, \mathrm{d}y\, G_{2\mathrm{D}} \frac{\delta n}{n_c} E_0.$$

However considering that E_0 is stronger in a narrow region along the cutoff, as it can be observed in Fig. 11, one can assume that the system shrinks to one dimension. Therefore in order to estimate the scattering efficiency, we take the 1D Green function [47]

$$G_{1\mathrm{D}}(y) = \frac{i\mathrm{e}^{ik|y|}}{2k}.$$

It introduces a k^{-1} dependency to the scattered field E_1, as well as to the scattering efficiency. Considering that the most of the contribution to the scattering comes from the point where E_0 is maximum (not exactly at the nominal cut-off), the scattering efficiency is proportional to k^{-1} at that point.

In the following part, k at the E_0 maximum is calculated analytically for O-mode. For slab geometry with a linear density profile and oblique incidence (following [48]) Eq. B.2 becomes

$$\frac{\partial^2 E_0}{\partial x^2} + k_0^2 \left(1 - \frac{x}{L} - \sin^2\theta\right) E_0 = 0$$

Using the transformation

$$\zeta = \left(\frac{k_0^2}{L}\right)^{1/3} (L\cos^2\theta - x),$$

the previous equation turns into

$$\frac{\partial^2 E_0}{\partial \zeta^2} + \zeta E_0 = 0. \tag{B.4}$$

Note that $\zeta = 0$ gives the nominal cut off, where the normal refractive index vanishes.

The solution to Eq. B.4 is given by the Airy function, which has an absolute maximum at $\zeta_{\max} \approx 1$. It is from this point (and not $\zeta = 0$) where the most of

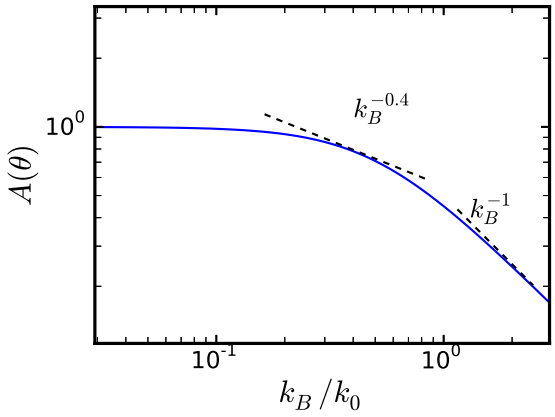

Figure B1. Scattering efficiency $A(\theta)$ as a function of k_B/k_0 computed from Eq. B.6. Two scalings with k_B are indicated in different regions.

the contributions to the backscattering comes. This is evidenced in Fig. 11 where the absolute maximum of the weighting function i.e. E_0 is slightly displaced from the nominal cutoff (dashed line). It corresponds to a position $x_{\max} = L\cos^2\theta - (L/k_0^2)^{1/3}$, where the wave number is

$$k = k_0\left[\left(\frac{1}{k_0 L}\right)^{2/3} + \sin^2\theta\right]^{1/2}. \tag{B.5}$$

The scattering efficiency correction factor is computed by normalizing k_0/k for normal incidence;

$$A(\theta) = \left[1 + \left(\frac{2\pi L}{\lambda_0}\right)^{2/3}\sin^2\theta\right]^{-1/2}. \tag{B.6}$$

In Fig. B1 the scattering efficiency $A(\theta)$ is plotted as a function of k_B/k_0 for the parameters used in this paper. It can be seen that, in the limit of large k_B the scattering efficiency scales as k_B^{-1}, this would mean that the measured spectral index can be underestimated by 1. In the limit of small k_B the scattering efficiency is constant, and in between both limits $A(\theta)$ scales with a k_B exponent in between 0 and 1. Fig. B1 depicts also a scaling $k_B^{-0.4}$ at an intermediate position.

The last derivation assumes a strong localization of the scattering along the cutoff, this is valid for the case under study as shown in Sec. 4.2. However in more general cases, contributions far from the cutoff may be important [44] and hence a more general approach is needed.

The previous calculation is not straight forward for X-mode. Here only an estimation is provided, it consists in approximating numerically the X-mode dispersion relation at the cut-off to

$$k^2 = k_0^2\left(1 - \frac{\omega_p^2}{\omega^2}\frac{\omega^2 - \omega_p^2}{\omega^2 - \omega_p^2 - \omega_c^2}\right) \approx k_0^2\left(\frac{L-x}{L^{\text{ref}}}\right),$$

where L^{ref} is the gradient scale length of the refractive index. L^{ref} can be used in Eq. B.6, instead of L. For the parameters in this paper it is found $L^{\mathrm{ref}} \approx 0.5L$. Notice that the last procedure is the same used to calculate the gradient scale length of the refractive index in Sec. 4.